Electronic Supplementary Material (ESI) for ChemComm.

This journal is © The Royal Society of Chemistry 2019

Electronic Supplementary Information

5.1% efficiency of Si photoanode for photoelectrochemical water splitting catalyzed by porous NiFe (oxy)hydroxide converted from NiFe oxysulfide

Wanyi Zhou,[a] Ronglei Fan,[a] Taozheng Hu,[a] Guanping Huang,[a] Weng Dong,[a] Xi Wu[b] and Mingrong Shen*[a]*

[a]*School of Physical Science and Technology, Jiangsu Key Laboratory of Thin Films, and Collaborative Innovation Center of Suzhou Nano Science and Technology, Soochow University, 1 Shizi street, Suzhou 215006, China*

[b]*College of Energy, Soochow University, 1 Shizi street, Suzhou 215006, China*

* Corresponding Author

E-mail: wuxi@suda.edu.cn

E-mail: mrshen@suda.edu.cn

Experimental section

The fabrication of n^+pp^+-Si electrodes

Single-crystalline p-Si wafers (156×156×0.18 mm^3, 1–3 Ω• cm specific resistance) were used in this work. The pyramid surface texture on both sides of silicon wafers was produced by chemical etching in a solution of KOH (Sigma, reagent grade) on a mass production line of crystalline-Si solar cells in the Suzhou company of Canadian Solar Inc. The as-prepared p-Si wafers were first covered with liquid phosphorus and boron dopant precursor by spin coating, respectively. Subsequently, to form an n^+ emitter layer and a p^+ electron back reflection layer for the p-Si, a thermal diffusion process was conducted at 950 ^{0}C for 180 min under the atmosphere of nitrogen in a diffusion furnace. After doping, an anti-reflection SiN_x layer and fritted Ag rod line were produced onto the n^+-Si emitter side. Finally, the samples were laser-cut into 1.5×1.5 cm^2. Such electrodes were then rinsed in deionized water which was degassed by ultrasonic clearing machine (i-Quip, Aladdin) and dried under a stream of N_2. We called such photoanode as n^+pp^+-Si. During PEC reaction, the light will be entering from n^+ side which was sealed on a transparent quartz substrate. The p^+ side will be loaded with the Ni protective layer and the NiFe related catalyst.

E-beam evaporation of the Ni layer on the Si surface

Before use, Si electrodes were cleaned by subsequent sonication in acetone, ethanol and water for 15 minutes each to remove any contaminants. The native SiO_2 layer on the p^+ side was then etched by dropping 5 wt % HF solution. A Ni layer was deposited on the Si surface via e-beam evaporation at a deposition rate of 0.5 Å s^{-1}. A layer thickness of ~10 nm was controlled and measured using the transmission electron microscope (TEM). Then, this Ni layer was partially activated in a three electrode PEC system to form a thin NiO_x layer on its surface. We called such electrode as n^+pp^+-Si/Ni/NiO_x. In detail, the Si/Ni electrode was activated by cycling the potential between 0.6 to 1.8 V_{RHE} using the cyclic voltammetry measurement for five times on the electrochemical workstation in 1.0 M NaOH electrolyte at the sweep rate of 5 mV/s

under simulated solar light (100mW/cm^2), with a Pt sheet as a counter electrode, Ag/AgCl (3M KCl) as a reference electrode and the n^+pp^+-Si/Ni as a working electrode.

Electrodeposition of the catalysts

The NiFe-S catalyst was electrodeposited on n^+pp^+-Si/Ni/NiO_x using the Ni layer as the working electrode, Pt wire as a counter electrode and Ag/AgCl (3M KCl) as a reference electrode. The deposition solution contains 5 mM $NiSO_4$, 1 mM $FeSO_4$ and 0.5 M thiourea in water. The potential of consecutive linear scan was cycled between -0.2 and 0.8 V_{RHE} at a scan rate of 5 mV/s under stirring. After deposition, the electrode was rinsed with copious water gently and dried under vacuum at room temperature overnight. This electrode was defined as n^+pp^+-Si/Ni/NiO_x/NiFe-S.

Then, we subjected the Si/Ni/NiO_x/NiFe-S to PEC measurements for ten times by cyclic voltammetry between 0.6 and 1.8 V_{RHE} under AM1.5G 1 sun illumination and 1M NaOH. The electrode was again rinsed with copious water gently and dried under vacuum at room temperature overnight. This electrode was defined as n^+pp^+-Si/Ni/NiO_x/NiFe-C. To make a comparison with the traditional NiFe (oxy)hydroxide, we also electrodeposited such catalyst using the same condition as that of NiFe-S except for the adding of thiourea in the deposition solution. After the deposition, the sample was also subjected to PEC measurements for ten times. This electrode was called as n^+pp^+-Si/Ni/NiO_x/NiFe.

PEC measurements

PEC measurements were conducted in a three-electrode cell configuration, using the Si photoanode as the working electrode, Ag/AgCl (3M KCl) as the reference electrode, and a Pt wire as the counter electrode. The potentials were controlled using an electrochemical workstation (Vertex, Ivium Technologies) and re-scaled to the potential according to the following equation: $V_{RHE} = V_{Ag/AgCl} + 0.197\ V + pH \times 0.059\ V$. A 300 W Xe lamp (Oriel, Newport Co.) with a silica filter to simulate solar light (AM1.5G illumination) was used as the light source. Before the PEC measurement, the

light intensity was carefully controlled at 100 mW/cm^2, measured using an optical power meter (Newport company) just before the light enters into the PEC cell. The performance of the photocathodes was measured using linear sweep voltammograms (LSVs) at 5 mV/s in a solution containing 1 M NaOH.

The solar-to-oxygen conversion efficiency (η) of a photoanode can be calculated based on the PEC current-potential curve like that of a solar cell, using equation: $\eta=J_{mp}(1.23V_{RHE}-V_{mp})/P_{in,}$ with J_{mp} and V_{mp} (V_{RHE}) are the photocurrent and potential at the maximum power point, respectively, and P_{in} as the power density of the illumination. It is assumed that there is no corrosion reaction at the photoelectrode, and a Faradaic efficiency of unity for both reactions.

To measure the stability of the photoelectrode, potential *vs.* time measurements were conducted at a constant current density of 40 mA/cm^2 for OER in 1 M NaOH solution under simulated AM1.5G illumination. The electrolyte was replaced and the sample was rinsed every 24h during the stability measurements.

The electrochemical impedance spectroscopy (EIS) curves were obtained at a constant 1.0 V_{RHE} using an electrochemical workstation (Vertex, Ivium Technologies) in the frequency range from 1 Hz to 100 MHz under illumination.

The Faradaic efficiency of the illuminated photoanodes was determined in a manner similar to the photocurrent measurements at a constant potential of 1.0 V_{RHE} and the amount of hydrogen produced on the Pt electrode was obtained using a gas chromatograph equipped with a thermal conductivity detector (Tianmei, GC 7900T).

Materials characterization

The surface morphology of the sample surface was analyzed using a field-emission scanning electron microscope (SEM) (SU8010, Hitachi). Transmission electron microscope (TEM) analysis was conducted by a Tecnai G220 (S-TWIN, FEI) operating at 200 kV. X-ray photoelectron spectroscopy (XPS) measurements were performed at room temperature using a spectrometer hemispherical analyzer (ESCALAB 250Xi, Thermo). All the binding energies were referenced to adventitious carbon at 284.6 eV.

The mechanism of the electrodeposition of NiFe-S.

Similar to the electrodeposition of Ni-Co-S (ACS Appl. Mater. Interfaces 2017, 9, 19746−19755), we proposed the overall reactions involved in the deposition of the NiFe-S catalyst are given below：

$$2H_2O + 2e^- \rightarrow 2OH^- + H_2 \quad (1)$$

$$SC(NH_2)_2 + 2OH \rightarrow S^{2-} + OC(NH_2)_2 + H_2O \quad (2)$$

$$Ni^{2+} + Fe^{2+} + S^{2-} \rightarrow NiFe\text{-}S \quad (3)$$

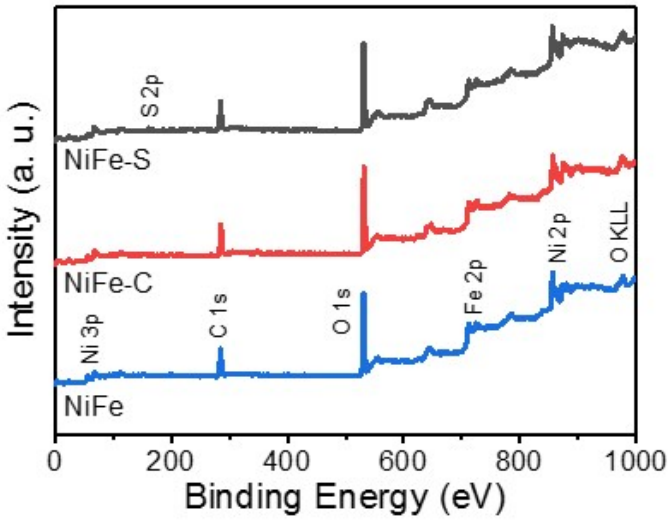

Fig. S1 Full XPS spectra of the NiFe, NiFe-C and NiFe-S deposited on $n^+pp^+Si/Ni/NiO_x$.

Table S1 Quantitative ratios of Ni^{2+} and Ni^{3+} in the NiFe and NiFe-C samples.

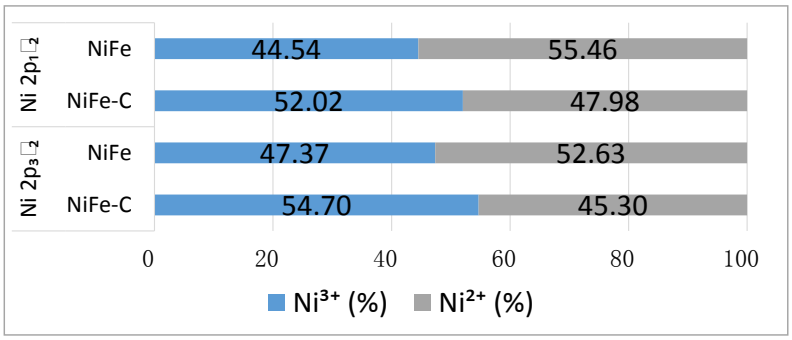

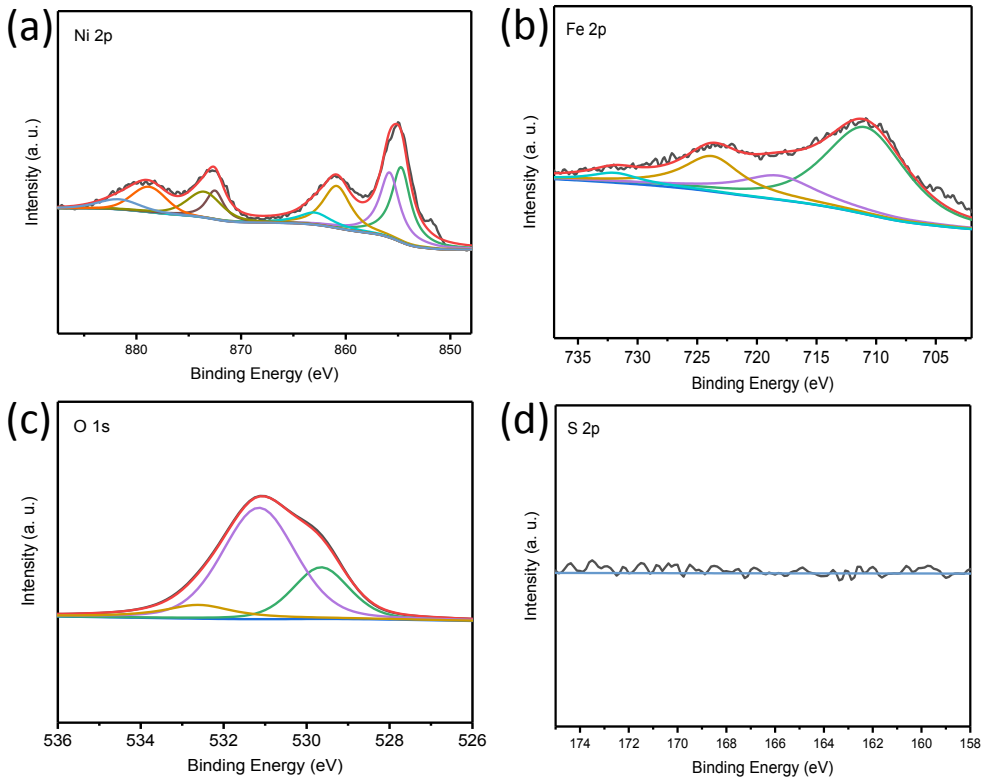

Fig. S2 High-resolution XPS spectra of (a) Ni 2p, (b) Fe 2p, (c) O 1s and (d) S 2p in Si/Ni/NiO_x/NiFe-C after etched ~10 nm on the electrode surface. There is also no S element inside the sample.

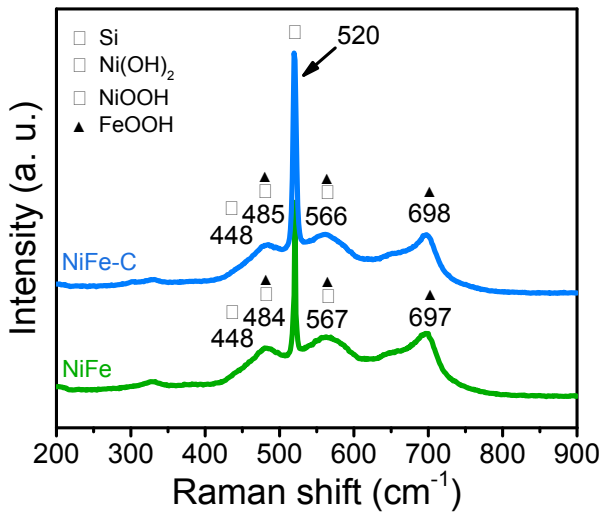

Fig. S3 Raman spectra for Si/Ni/NiOx/NiFe and Si/Ni/NiOx/NiFe-C. No significance

changes were found. The peak at 448 cm^{-1} is assigned to $Ni(OH)_2$, the peaks at around 486 cm^{-1} and 566 cm^{-1} are both attributed to NiOOH and FeOOH and the peak at 698 cm^{-1} is attributed to FeOOH.

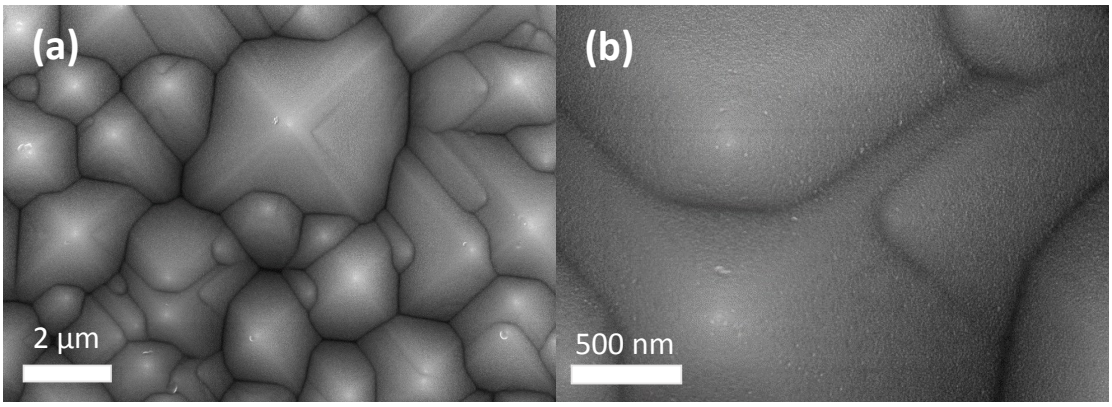

Fig. S4 The SEM images of Si/Ni/NiO_x on the MP textured Si surface. The Ni layer deposited via e-beam evaporation is quite dense and smooth.

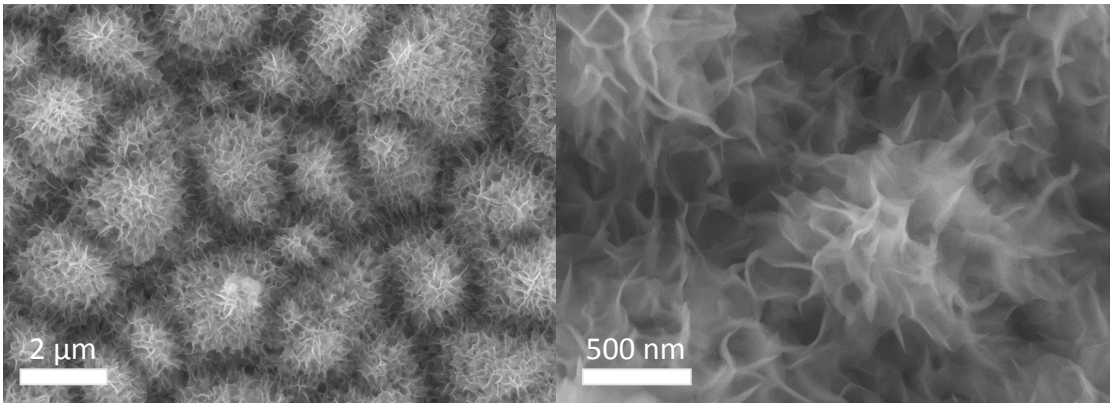

Fig. S5 The SEM surface images of Si/Ni/NiO_x/NiFe-S. Right picture is the enlarged one.

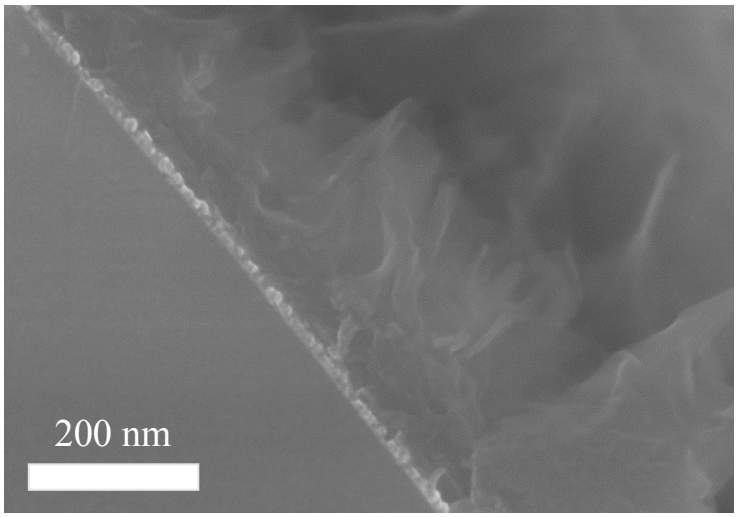

Fig. S6 The enlarged view from Fig. 2c.

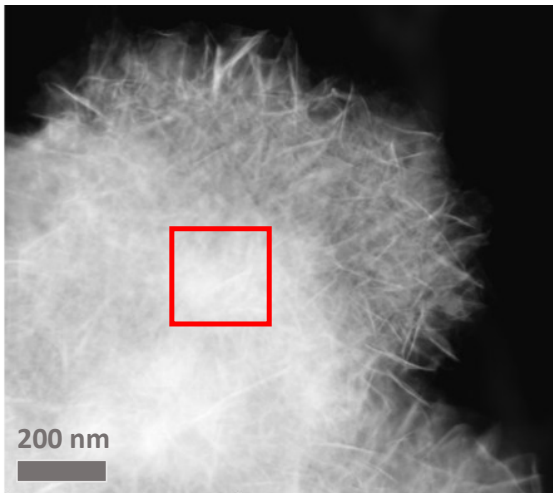

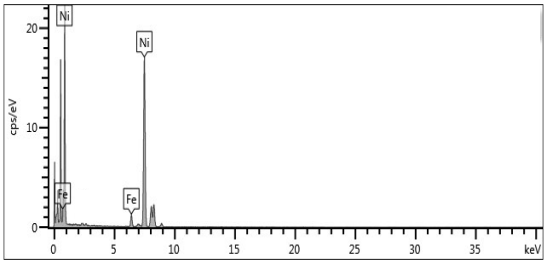

Element	wt%	at%
Fe	5.85	6.13
Ni	94.15	93.87

Fig. S7 The Energy Dispersive X-Ray Spectroscopy (EDS) results for NiFe-C. The mole ratio of Fe/Ni is determined to be 6.5%.

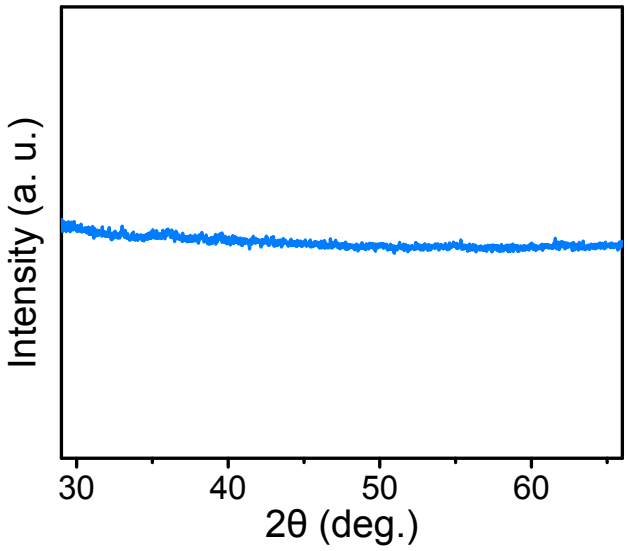

Fig. S8 X-ray diffraction (XRD) spectrum of NiFe-C. No diffraction peaks were observed in the XRD spectrum, suggesting the poor crystallinity of the catalysts.

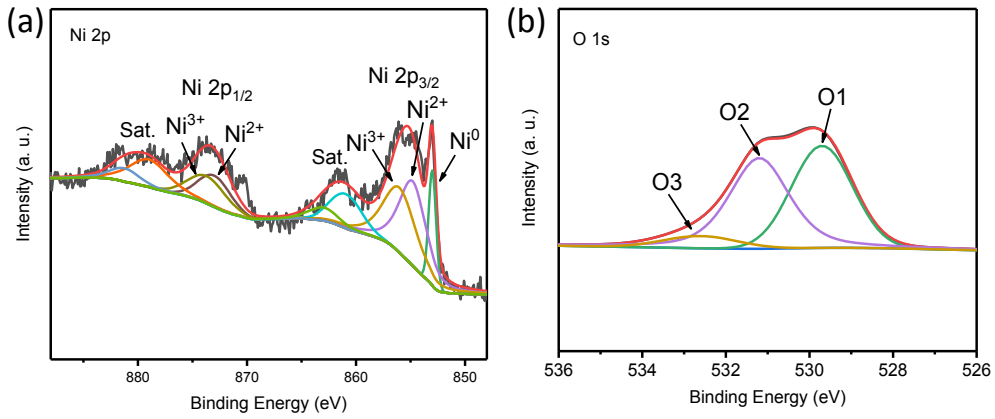

Fig. S9 High-resolution XPS spectra of (a) Ni 2p and (b) O 1s on the Si/Ni/NiO_x surface, showing the formation of NiO_x.

Fig. S10 EDS elemental mapping of element S for Si/Ni/NiO_x/NiFe-C.

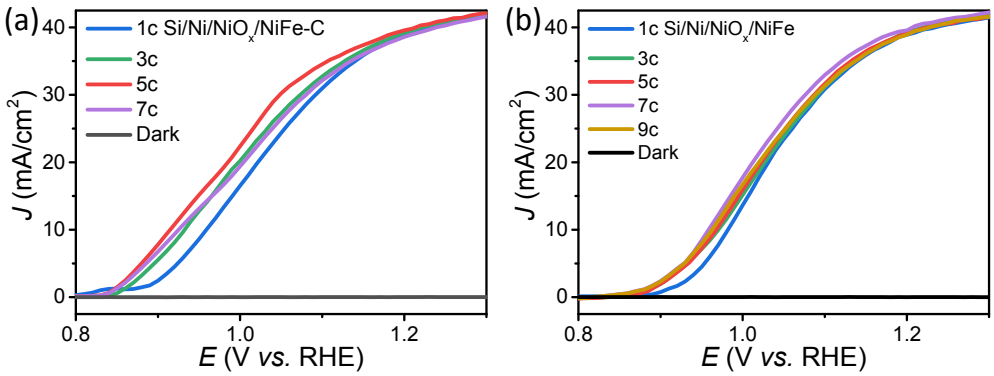

Fig. S11 (a) PEC *J-V* curves of Si/Ni/NiO_x/NiFe-C (a) and Si/Ni/NiO_x/NiFe (b) with different deposition cycles. Si/Ni/NiO_x/NiFe-C (5 cycles) shows the best PEC-OER activity, while that for Si/Ni/NiO_x/NiFe is 7 cycles.

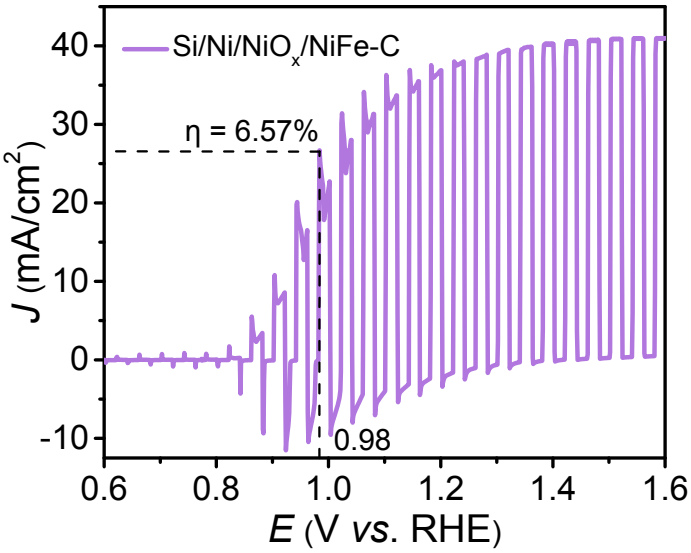

Fig. S12 PEC J-V curve of NiFe-C under chopped illumination. Conversion efficiency η can reach up to 6.5%.

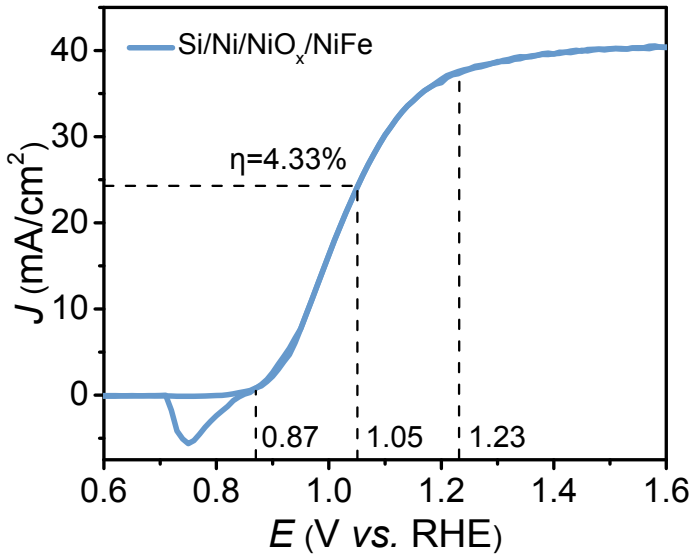

Fig. S13 The PEC performance of Si/Ni/NiO$_x$/NiFe photoanode. An onset potential of 0.87 V_{RHE} and an energy conversion efficiency of 4.33% at 1.05 V_{RHE} can be obtained.

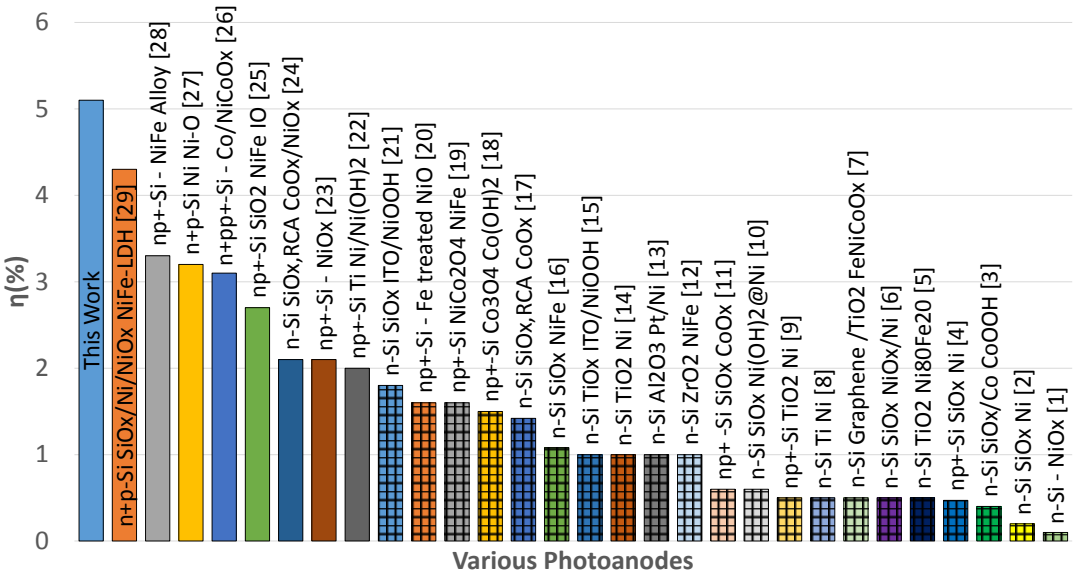

Fig. S14 Comparison of the energy conversion efficiency for the reported Si-based photoanodes with the current one.

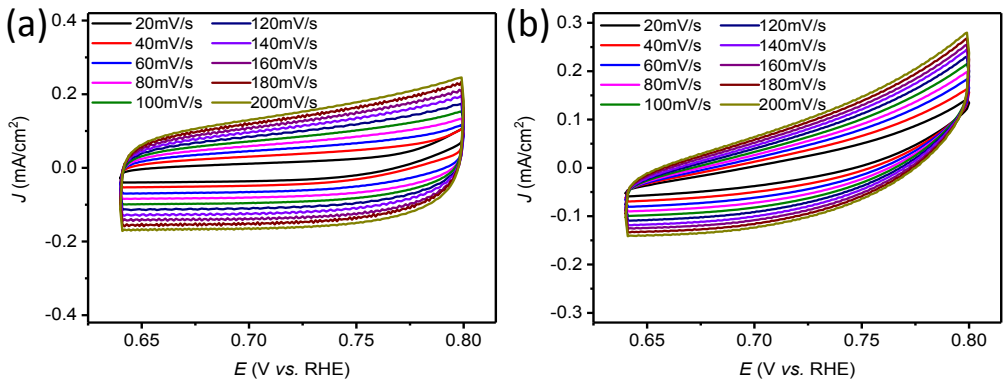

Fig. S15 Typical CV curves of (a) Si/Ni/NiO_x/NiFe-C and (b) Si/Ni/NiO_x/NiFe.

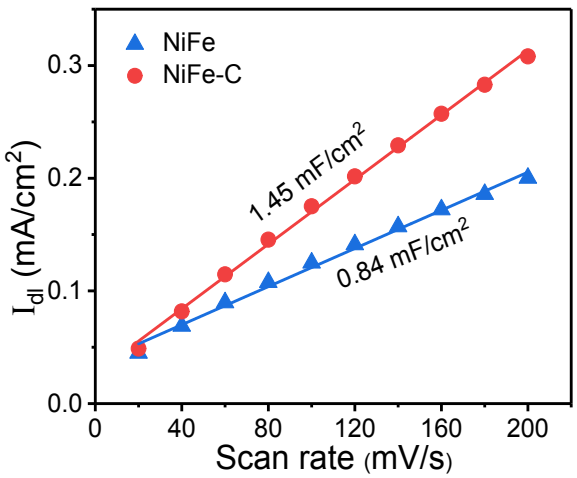

Fig. S16 Capacitive currents I_{dl} of Si/Ni/NiO_x/NiFe-C and Si/Ni/NiO_x/NiFe at 0.725 V_{RHE} as a function of the scan rate.

Electrochemical capacitance was measured using cyclic voltammetry (CV) measurements in dark. The currents were measured in a narrow potential window (0.65-0.80 V_{RHE}) that no faradaic processes were observed. CVs were collected at different scan rates: 20, 40, 60, 80, 100, 120, 140, 160, 180 and 200 mV/s. The measured current in this non-faradaic potential region should be mostly due to the charging of the double-layer. The capacitive current was the difference values between two currents at 0.725 V_{RHE}.

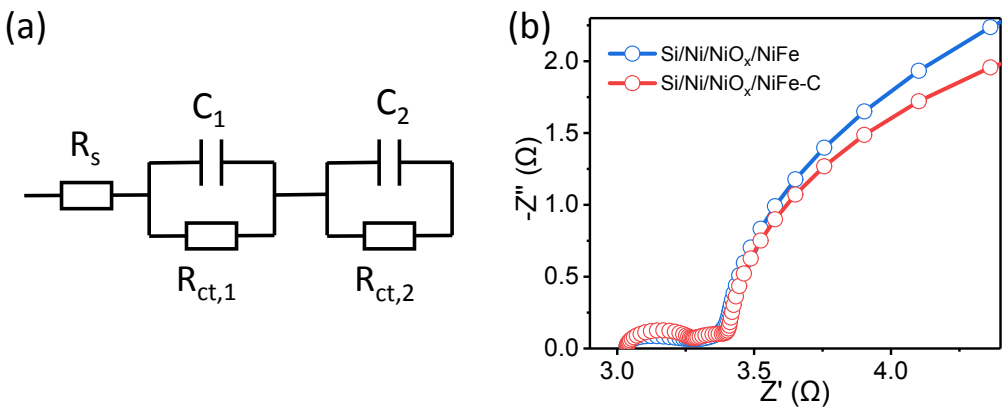

Fig. S17 (a) Equivalent circuits for Si/Ni/NiO_x/NiFe and Si/Ni/NiO_x/NiFe-C and (b) the corresponding EIS Nyquist plots.

R_s represents series resistance of the whole circuit. $R_{ct,1}$ represents charge-transfer resistance from Si photoelectrode to catalyst and C_1 is the capacitance of the corresponding Si photoelectrode/catalyst junction, $R_{ct,2}$ represents the charge-transfer resistance from the NiFe or NiFe-C catalyst to the electrolyte and C_2 is the capacitance of the corresponding catalyst/electrolyte junction.

Table S2 Fitting EIS data for the NiFe-C and NiFe using the equivalent circuit.

	NiFe-C	NiFe
$R_s(\Omega)$	3.056	3.551
$R_{ct,1}(\Omega)$	0.031	0.260
$R_{ct,2}(\Omega)$	4.803	5.999

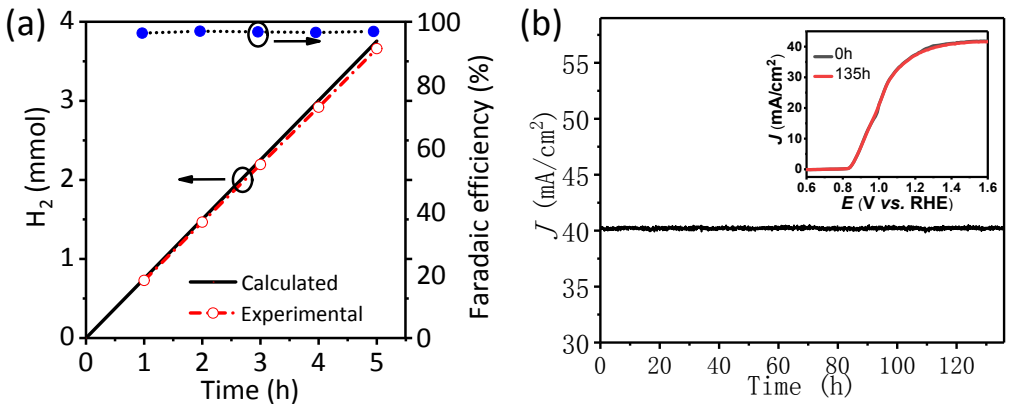

Fig. S18 (a) H_2 production on time and the corresponding Faradic efficiency for Si/Ni/NiO_x/NiFe-C. (b) PEC stability measurement for Si/Ni/NiO_x/NiFe-C biased at 1.2 V_{RHE} in 1M NaOH solution under 100 mW/cm^2 Xe lamp. The inset is the J-V curves before and after 135 h PEC reaction.

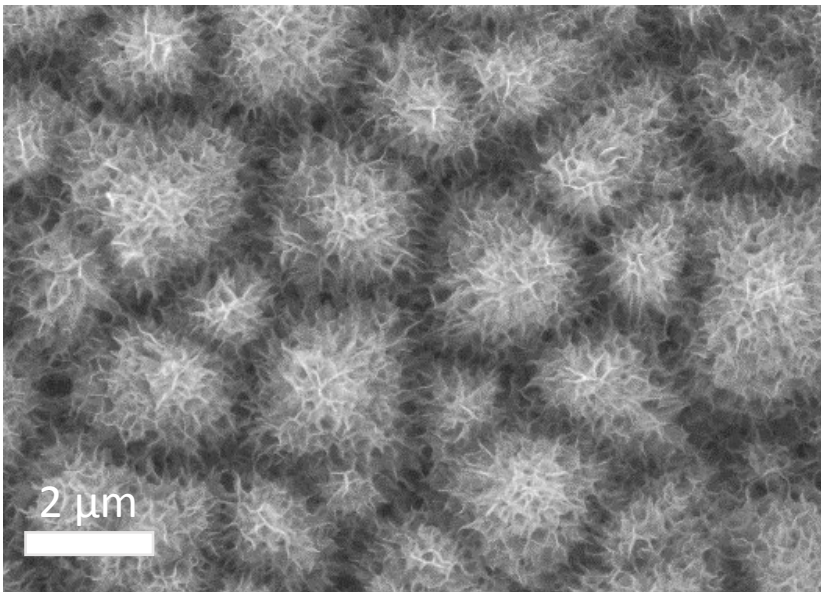

Fig. S19 SEM surface morphology of Si/Ni/NiO_x/NiFe-C after 135 h PEC reaction.

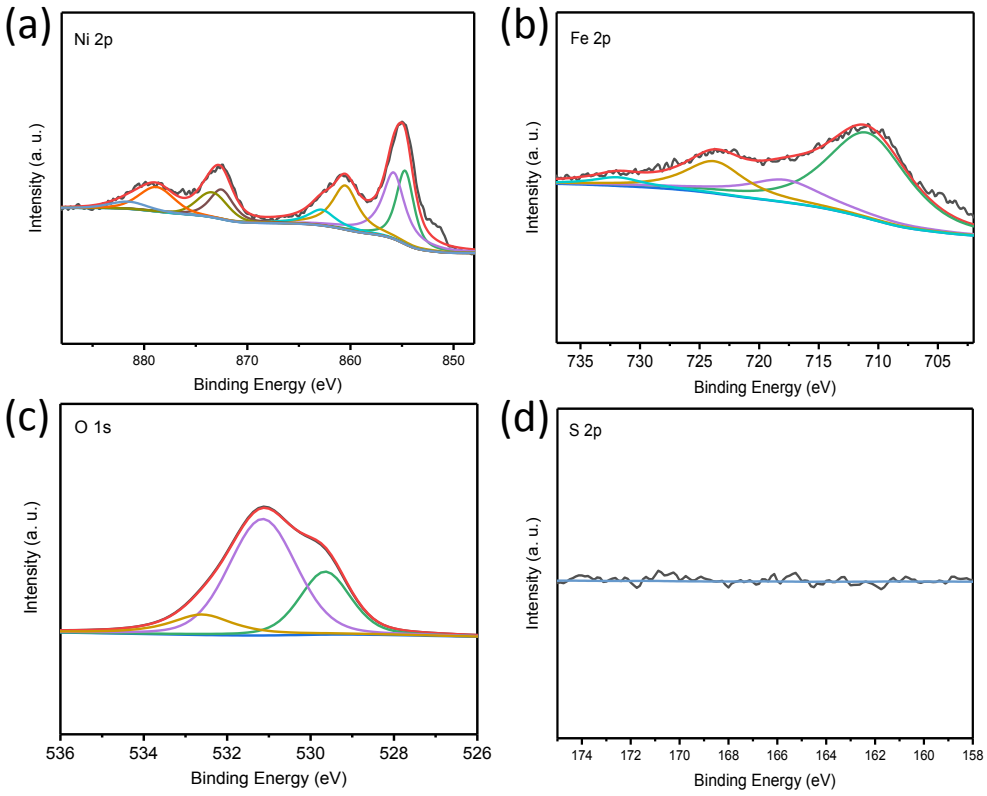

Fig. S20 High-resolution XPS spectra of (a) Ni 2p, (b) Fe 2p and (c) O 1s, and (d) S 2p of Si/Ni/NiO_x/NiFe-C after 135 h PEC reaction.

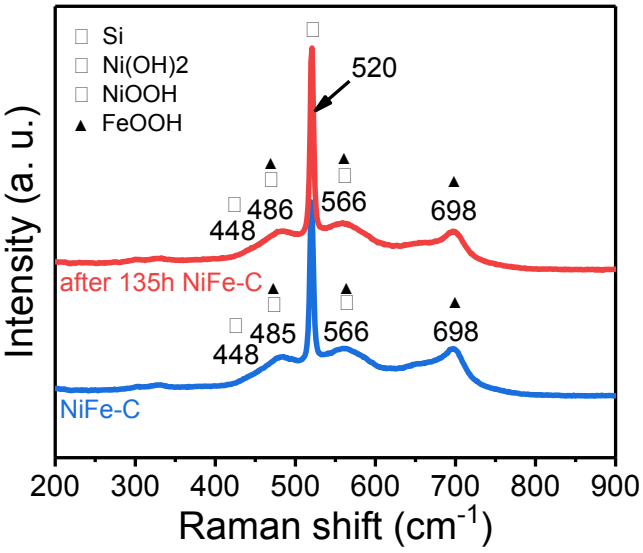

Fig. S21 Raman spectra before and after the135h testing for Si/Ni/NiO_x/NiFe-C.

references

1 K. Sun, N. Park, Z. Sun, J. Zhou, J. Wang, X. Pang, S. Shen, S. Y. Noh, Y. Jing, S. Jin, P. K. L. Yu and D. Wang, *Energy Environ. Sci.*, 2012, **5**, 7872.

2 M. J. Kenney, M. Gong, Y. Li, J. Z. Wu, J. Feng, M. Lanza and H. Dai, *Science*, 2013, **342**, 836.

3 J. C. Hill, A. T. Landers and J. A. Switzer, *Nat. Mater.*, 2015, **14**, 1150.

4 K. Sun, N. L. Ritzert, J. John, H. Tan, W. G. Hale, J. Jiang, I. Moreno-Hernandez, K. M. Papadantonakis, T. P. Moffat, B. S. Brunschwig and N. S. Lewis, *Sustainable Energy Fuels*, 2018, **2**, 983.

5 Q. Cai, W. Hong, C. Jian, J. Li and W. Liu, *ACS Catal.*, 2017, **7**, 3277.

6 S. A. Lee, T. H. Lee, C. Kim, M. G. Lee, M.-J. Choi, H. Park, S. Choi, J. Oh and H. W. Jang, *ACS Catal.*, 2018, **8**, 7261.

7 C. Li, Y. Xiao, L. Zhang, Y. Li, J.-J. Delaunay and H. Zhu, *Sustainable Energy Fuels*, 2018, **2**, 663.

8 Y. Shi, T. Han, C. Gimbert-Surinach, X. Song, M. Lanza and A. Llobet, *J. Mater. Chem. A*, 2017, **5**, 1996.

9 S. Hu, M. R. Shaner, J. A. Beardslee, M. Lichterman, B. S. Brunschwig and N. S. Lewis, *Science*, 2014, **344**, 1005-1009.

10 G. Xu, Z. Xu, Z. Shi, L. Pei, S. Yan, Z. Gu and Z. Zou, *ChemSusChem*, 2017, **10**, 2897.

11 J. Yang, K. Walczak, E. Anzenberg, F. M. Toma, G. Yuan, J. Beeman, A. Schwartzberg, Y. Lin, M. Hettick, A. Javey, J. W. Ager, J. Yano, H. Frei and I. D. Sharp, *J. Am. Chem. Soc.*, 2014, **136**, 6191.

12 Q. Cai, W. Hong, C. Jian, J. Li and W. Liu, *ACS Catal.*, 2018, **8**, 9238.

13 I. A. Digdaya, G. W. P. Adhyaksa, B. J. Trzesniewski, E. C. Garnett and W. A.

Smith, *Nat. Commun.*, 2017, **8**, 15968.
14 L. Gao, Q. Li, H. Chen, S. Hayase and T. Ma, *Sol. RRL*, 2017, **1**, 1700064.
15 T. Yao, R. Chen, J. Li, J. Han, W. Qin, H. Wang, J. Shi, F. Fan and C. Li, *J. Am. Chem. Soc.*, 2016, **138**, 13664.
16 C. Li, M. Huang, Y. Zhong, L. Zhang, Y. Xiao and H. Zhu, *Chem. Mater.*, 2018, **31**, 171.
17 X. Zhou, R. Liu, K. Sun, K. M. Papadantonakis, B. S. Brunschwig and N. S. Lewis, *Energy Environ. Sci.*, 2016, **9**, 892.
18 J. Yang, J. K. Cooper, F. M. Toma, K. A. Walczak, M. Favaro, J. W. Beeman, L. H. Hess, C. Wang, C. Zhu, S. Gul, J. Yano, C. Kisielowski, A. Schwartzberg and I. D. Sharp, *Nat. Mater.*, 2016, **16**, 335.
19 L. Chen, J. Yang, S. Klaus, L. J. Lee, R. Woods-Robinson, J. Ma, Y. Lum, J. K. Cooper, F. M. Toma, L. W. Wang, I. D. Sharp, A. T. Bell and J. W. Ager, *Journal of the American Chemical Society*, 2015, **137**, 9595.
20 B. Mei, A. A. Permyakova, R. Frydendal, D. Bae, T. Pedersen, P. Malacrida, O. Hansen, I. E. L. Stephens, P. C. K. Vesborg, B. Seger and I. Chorkendorff, *J. Phys. Chem. Lett.*, 2014, **5**, 3456.
21 S. Yoon, J.-H. Lim and B. Yoo, *Electrochim. Acta*, 2017, **237**, 37.
22 S. Oh and J. Oh, *J. Phys. Chem. C*, 2015, **120**, 133.
23 K. Sun, M. T. McDowell, A. C. Nielander, S. Hu, M. R. Shaner, F. Yang, B. S. Brunschwig and N. S. Lewis, *J. Phys. Chem. Lett.*, 2015, **6**, 592.
24 X. Zhou, R. Liu, K. Sun, D. Friedrich, M. T. McDowell, F. Yang, S. T. Omelchenko, F. H. Saadi, A. C. Nielander, S. Yalamanchili, K. M. Papadantonakis, B. S. Brunschwig and N. S. Lewis, *Energy Environ. Sci.*, 2015, **8**, 2644.
25 S. Oh, H. Song and J. Oh, *Nano Lett.*, 2017, **17**, 5416.
26 D. Bae, B. Mei, R. Frydendal, T. Pedersen, B. Seger, O. Hansen, P. C. K. Vesborg and I. Chorkendorff, *ChemElectroChem*, 2016, **3**, 1546.
27 G. Huang, R. Fan, X. Zhou, Z. Xu, W. Zhou, W. Dong and M. Shen, *Chem. Commun.*, 2019, **55**, 377.
28 X. Yu, P. Yang, S. Chen, M. Zhang and G. Shi, *Adv. Energy Mater.*, 2017, **7**, 1601805.
29 B. Guo, A. Batool, G. Xie, R. Boddula, L. Tian, S. U. Jan and J. R. Gong, *Nano Lett.*, 2018, **18**, 1516.